Spectroscopic characterization of hydroxyquinoline derivatives with bromine and iodine atoms and theoretical investigation by DFT calculations, MD simulations and molecular docking studies

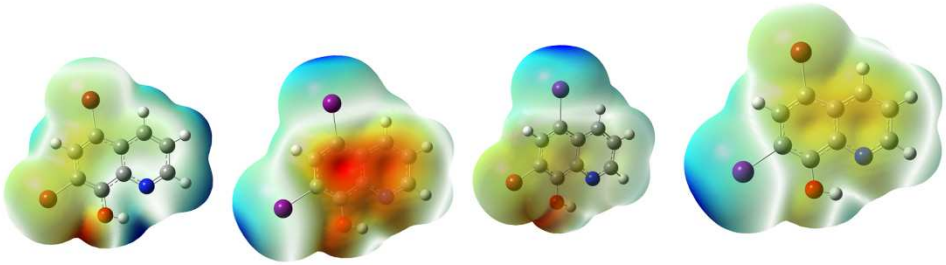

Spectroscopic characterization of hydroxyquinoline derivatives with bromine and iodine atoms and theoretical investigation by DFT calculations, MD simulations and molecular docking studies

B.Sureshkumar[a], Sheena MaryY[b*], K.S. Resmi[b], S.Suma[a], Stevan Armaković[c], Sanja J. Armaković[d], C. Van Alsenoy[e], B.Narayana[f], D.Sobhana[a]

[a]Department of Chemistry, SN College, Kollam, Kerala, India

[b]Department of Physics, Fatima Mata National College, Kollam, Kerala, India

[c]University of Novi Sad, Faculty of Sciences, Department of Physics, Trg D. Obradovića 4, 21000 Novi Sad, Serbia

[d]University of Novi Sad, Faculty of Sciences, Department of Chemistry, Biochemistry and Environmental Protection, Trg D. Obradovića 3, 21000 Novi Sad, Serbia

[e]Department of Chemistry, University of Antwerp, Groenenborgerlaan 171, B-2020, Antwerp, Belgium

[f]Department of Chemistry, Mangalore University, Mangalagangothri, Mangaluru, Karnataka, India

* Corresponding Author:email: sypanicker@rediffmail.com

Abstract: In the present work, spectroscopic characterization of 5,7-dibromo-8-hydroxy quinoline (DBHQ(1)) and 5,7-diiodo-8-hydroxy quinoline (DIHQ(2)) has been obtained theoretically and experimentally. On the basis of potential energy distribution of vibrational modes, complete assignments of wavenumbers were performed yielding good agreement between experimental and theoretical wavenumbers. The HOMO-LUMO plots in the title molecules show the charge transfer in the molecular system through the conjugated paths. The electrophilic and nucleophilic sites are revealed from the molecular electrostatic potential maps. Experimental investigation encompassed spectroscopic characterization by FT-IR and Raman techniques while computational studies included DFT calculation, molecular dynamics (MD) simulations and molecular docking studies. MD simulations provided insights into the reactivity with water and with selected proteins. The molecular docking studies reveal that the ligands bind at the active site of the macromolecule and could restrict or block the functioning of Plasmodium falciparum

dihydrofolatereductase-thymidylate synthase (PfDHFR-TS), there by acting as antiprotozoal agents. Drug activity and binding affinity of halogen positional changes in the title molecules with target protein were reported and this study thesaurus the effects of bio-efficiency in the molecule.

Keywords: DFT; Quinoline; MD; Docking; ALIE; RDF.

1. Introduction

Derivatives of quinoline are pharmaceutically and biologically important heterocyclic molecules containing a benzene and pyridine rings fused together at nearby two side carbon atoms. In general, quinoline-based molecules are widely used as a source for the synthesis of numerous drugs with anti-bacterial [1], anti-filarial [2], anti-malarial [3], anti-fungal [4], cardiovascular [5], anti-tuberculosis [6], local anesthesia [7], anti-neoplastic [8] activities, while in the same time they can be used as receptor agonists. Aside of their pharmaceutical importance, quinoline derivatives are also important in the area of materials science, especially for the development of novel OLED devices [9-12]. Among others, these molecules are of importance for LED materials based on polymers [13], while some other representatives of these molecules are able to produce sharp green electroluminescence with significant quantum efficiency of emission in blue and green spectral areas region [12, 14]. Quinoline derivative's non-centro symmetry is used for the synthesis of materials with non-linear response (NLO molecules) [15]. Besides, they are used for production of optical switching devices [16], photographic sensitizers and electrochemical sensing devices [17]. Lakshmi et al. [18] reported the spectroscopic studies of hydroxyquinoline derivatives experimentally and theoretically. Taking into account the importance of computational studies for the investigation of various properties of organic molecules [19-22], in the present study of quinoline derivatives we have applied both DFT and MD approaches. Global reactive properties have been investigated by visualization of frontier molecular orbitals and by calculation of well-established quantum molecular descriptors. Surfaces of molecular electrostatic potential (MEP) and average local ionization energies (ALIE) have been obtained in order to assess the reactive properties based on the charge distribution, while Fukui functions also served for identification of possibly important reactive molecular sites. Understanding of degradation properties of pharmaceutical molecules is of great importance from the

ecological aspects, since natural weather conditions are usually not enough for their degradation [23-25]. Oxidative processes are of great importance for degradation of organic molecules [24, 26-31] and in this regard we have also calculated bond dissociation energies (BDE) for hydrogen atoms, since these quantities are connected with molecule's sensitivity towards autoxidation mechanism. Hydrolysis mechanism is also important since pharmaceutical molecules eventually end up in some type of water. Therefore, in order to understand molecules stability in water, MD simulations have been performed with the latest OPLS3 force field.

2. Experimental Details

Fine samples of the title compounds were obtained from Sigma Aldrich chemical company, USA and used without any further purification for spectral measurements. The FT-IR and FT-Raman spectra (Figs.S1 and S.2-supporting information) were recorded using Perkin-Elmer spectrum RX1 and Nicolet model 950 FT-Raman spectrometers.

3. Computational Details

Calculations of the wavenumbers, polarizability values, frontier molecular orbital analysis were carried out with Gaussian 09 program [32] using the B3LYP/SDD quantum chemical calculation method. A scaling factor of 0.9613 is used to scale the theoretically obtained wavenumbers [33] and the assignments of the vibrational wavenumbers are done by using GaussView [34] and GAR2PED software [35]. Jaguar 9.7 [36] program and Desmond [37-40] program have been also used for computational investigation of the quinoline derivatives. Namely, Jaguar was used for DFT calculations, while Desmond was used for MD simulations, both as implemented in Schrödinger Materials Science Suite 2017-3. B3LYP exchange-correlation functional [41] has been employed for DFT calculations with Jaguar, with 6-311++G(d,p), 6-31+G(d,p) and 6-311G(d,p) basis sets, for the calculations of ALIE, Fukui functions and BDEs, respectively. OPLS3 [37, 42-44] force field was employed for MD simulations. Simulation time was set to 10 ns, while temperature was set to 300 K. Pressure was 1.0325 bar, while cut off radius was 10 Å. System was of isothermal–isobaric (NPT) ensemble class, with simple point charge (SPC) model [45] used for the description of solvent. System was modeled by placing of one target molecule into the cubic box with ~2000 water molecules. The method of Johnson et al. [46, 47] was used, as implemented in Jaguar program, for the

determination and characterization of noncovalent interactions. Maestro GUI [48] was used for the preparation of input files and analysis of results in the case of Jaguar and Desmond programs.

4. Results and discussion

4.1 IR and Raman spectra

The rings, C1-C2-C3-C4-C5-C6 and C4-C5-C10-C9-C8-N7 are designated as PhI and PhII, respectively, in the following discussion (Fig.1). The vibrational assignments of the title compounds are given in table 1. The modes at 3090 cm^{-1} (PhI), 3083, 3067, 3037 cm^{-1} (PhII) (DFT) and at 3123 cm^{-1} (PhI) and 3122, 3100, 3088 cm^{-1} (PhII) (DFT) are assigned as the CH stretching modes of DBHQ(**1)** and DIHQ(**2)** [49, 50] and these modes are observed at 3070 cm^{-1} (IR) and 3130, 3105, 3085, 3070, 3067, 3040 cm^{-1} (Raman). DFT calculations give the ring stretching modes of DBHQ(**1)** and DIHQ(**2)**, at 1585, 1537, 1461, 1363, 1313 cm^{-1} for PhI, 1568, 1537, 1428, 1346, 902 cm^{-1} for PhII and at 1587, 1528, 1454, 1420, 1348 cm^{-1} for PhI, 1560, 1420, 1361, 1239, 879 cm^{-1} for PhII [51]. Experimentally these ring stretching modes are observed at 1583, 1459, 1365, 1320 cm^{-1} (PhI), 1570 (PhII) cm^{-1} in the IR spectrum, 1584, 1540, 1460, 1365, 1315 (PhI), 1566, 1540, 1430, 1344, 899 cm^{-1} (PhII) in the Raman spectrum for DBHQ(**1)** and at 1590, 1531, 1453, 1340 cm^{-1} (PhI), 1558, 1364, 1241 (PhII) cm^{-1} in the IR spectrum, 1590, 1453, 1342 (PhI), 1559, 1361, 1242 (PhII) cm^{-1} in the Raman spectrum for DIHQ(**2)**. For poly substituted phenyl rings, the ring breathing mode is reported at 1006 cm^{-1} (IR) and at 998 cm^{-1} (DFT) [52] and at 1003 cm^{-1} (DFT) [53] and for DBHQ(**1)** and DIHQ**(2),** the ring breathing modes are assigned at 1021 and 1018 cm^{-1}(DFT). In the present case, the bands at 1210 cm^{-1} (IR), 1213 cm^{-1} (Raman), 1215 cm^{-1} (DFT) for PhI, 1244, 1125 (IR), 1244, 1177, 1125 (Raman), 1243, 1175, 1115 cm^{-1} (DFT) for PhII and 1189 cm^{-1} (IR), 1185 (Raman) 1186 cm^{-1} (DFT) for PhI, 1227, 1120 (IR), 1226, 1159, 1120 (Raman), 1222, 1162, 1117 cm^{-1} (DFT) for PhII are assigned as the in-plane CH deformations of the title compounds, DBHQ(**1)** and DIHQ(**2)**, respectively. The out-of-plane CH deformation modes are assigned at 857, 930, 789 cm^{-1} (IR), 955, 925, 860, 782 (Raman), 953, 925, 855, 780 cm^{-1} (DFT) for DBHQ(**1)** and at 988, 949, 903, 838 cm^{-1} (IR), 996, 840 cm^{-1} (Raman), 999, 951, 900, 833 cm^{-1} (DFT) for DIHQ(**2)**, respectively. According to literature [53], for tetra-substituted benzenes, a strong band is seen in 850-

840 cm^{-1} due to out-of-plane CH deformation and in the present case this mode appears at 855 and 835 cm^{-1}.

Quinoline ring stretching modes are reported at 1563 cm^{-1} (IR), 1560 cm^{-1} (Raman) and 1568 cm^{-1} (DFT) (C=C stretching mode), 1500 cm^{-1} (Raman) and 1527 cm^{-1} (DFT) (C=N stretching), 1281 cm^{-1} (IR), 1285 cm^{-1} (Raman) and 1285 cm^{-1} (DFT) (C-N stretching), 1476 cm^{-1} (IR), 1205 cm^{-1} (Raman), 1204 and 1474 cm^{-1} (DFT) (C-C stretching modes) [54]. The bands at 1388 (IR), 1384 cm^{-1} in the Raman spectrum, 1381 cm^{-1} (DFT) and 1384 (IR), 1381 cm^{-1} in the Raman spectrum, 1380 cm^{-1} (DFT) are assigned as the in-plane OH deformation modes for DBHQ(**1)** and DIHQ(**2)**, respectively [51]. The stretching of hydroxyl group C-O appears at 1181 cm^{-1} (DFT) for DBHQ(**1)** and 1186 cm^{-1} (DFT) for DIHQ(**2)** [55, 56]. The out-of-plane deformation is expected generally in the region 650±80 cm^{-1} [51] and in the present case it is assigned at 601 and 662 cm^{-1} (DFT) for DBHQ(**1)** and DIHQ(**2)**, respectively. The C-Br stretching vibration was reported at 617 cm^{-1} experimentally and at 616 cm^{-1} theoretically by Arshad et al. [57]. Zainurit et al. [58] reported the C-I stretching mode at 317 cm^{-1} theoretically. The CBr and CI stretching modes of the title compound are assigned at 658, 646 cm^{-1} and 282, 248 cm^{-1}, respectively as expected.

4.2 ALIE surface, Fukui functions and noncovalent interactions

We have mapped ALIE values to the electron density surface in order to clearly detect molecule sites where electrons are least tightly bonded and therefore the molecule sites that are prone to electrophilic attacks [59-62]. Representative ALIE surfaces of two investigated quinoline derivatives have been presented in Fig.2. ALIE surfaces of DBHQ(**1)** and DIHQ(**2)** provided in Fig.2 indicate that locations of bromine and iodine atoms are characterized by the lowest ALIE values and therefore it can be concluded that these molecule sites are prone to electrophilic attacks. However, it can be also seen that the lowest ALIE value of DIHQ(**2)** is much lower, for ~18 kcal/mol, than the lowest ALIE value of DBHQ(**1)**, thus indicating that quinoline derivative with iodine atoms is much more sensitive towards electrophilic attacks. Maximal ALIE values (~382 kcal/mol) are in both cases located in the near vicinity of hydrogen atom of OH group, indicating location where electrons are the most tightly bonded to the molecules. It is also interesting to note that the lowest ALIE value of derivative with iodine atoms is

practically matching the lowest ALIE value of the pristine quinoline, which we have reported earlier [28].

Analysis of electron density between atoms of DBHQ(**1)** and DIHQ(**2)** reveals formation of several noncovalent interactions (Fig.3) within quinoline derivative with iodine atoms. Namely, in the case of DIHQ(**2)** four noncovalent interactions have been determined, with the strongest one being between iodine and adjacent carbon atoms (with corresponding strengths of –0.089 electron/bohr^3). Other two noncovalent interactions in the case of DIHQ(**2)** involve iodine I12 and carbon C10 atoms, which is the weakest noncovalent interaction, and nitrogen N7 and hydrogen H18 atoms. Only one noncovalent interaction formed in the case of DBHQ(**1)**, between nitrogen N7 and H18 atoms, with the same strength as the corresponding noncovalent interaction in the case of DIHQ(**2)**.

In this study Fukui functions have been calculated according to the following equations:

$$f^{+} = \frac{\left(\rho^{N+\delta}(r) - \rho^{N}(r)\right)}{\delta}, \quad (1)$$

$$f^{-} = \frac{\left(\rho^{N-\delta}(r) - \rho^{N}(r)\right)}{\delta}, \quad (2)$$

where *N* stands for the number of electrons in reference state of the molecule, while δ stands for the fraction of electron which default value is set to be 0.01 [63]. The values of calculated Fukui functions have been mapped to the electron density surface, in order to visualize locations where electron density increased/decreased after the addition/removal of charge (Fig.4).

Positive color in Fig.4 in the case of Fukui f^{+} functions is the purple one, and indicates molecule sites where electron density increases after the charge addition. On the other side negative color is the red one and in the case of f^{-} functions indicates molecule sites where electron density decreased after the removal of charge. In terms of position of positive color in the case of f^{+} functions it can be seen that quinoline derivatives are very similar. Namely, in both cases purple color of f^{+} function is located at two specific sites of the nitrogen containing six member ring (carbon atoms C8 and C10), designating them as the electrophilic molecule sites where electron density increases after the addition of

charge. On the other side, although distribution of positive color in the case of f^- function differs significantly, the location of negative color which determines where electron density decreased after the removal of charge is again practically the same for both quinoline derivatives. Namely, in the case of f^- function for both moelcules negative color is located in the near vicinity of carbon atom C5.

4.3 Reactive and degradation properties based on autoxidation and hydrolysis

Computational investigations of organic molecules based on DFT calculations and MD simulations are of great importance for the understanding of their reactive properties [64-67]. Taking into account how oxidation reactions are important as degradation pathways of pharmaceuticals and organic materials [68], in this work we have calculated BDE for hydrogen abstraction (H-BDE), since this quantity can indicate whether some organic molecule is sensitive or not towards autoxidation mechanism [68-70]. H-BDE values between 70 and 85 kcal/mol [71, 72] indicate sensitivity towards autoxidation mechanism. H-BDE values between 85 and 90 kcal/mol could also be of importance for autoxidation mechanism, but should be treated with caution [72], while H-BDE values lower than 70 kcal/mol are not appropriate for autoxidation mechanism [19, 71, 73]. Fig.5 contains information about BDE values for all single acyclic bonds of DBHQ(**1)** and DIHQ(**2)**.

H-BDE values provided in Fig.5 indicate that both quinoline derivatives are highly stable towards autoxidation mechanism. This also indicates that their degradation under natural conditions is hard and imposes the necessity of advanced oxidation processes for their efficient removal. The lowest H-BDE value of ~93 kcal/mol for both derivatives is located on the hydrogen atom of OH group, however this is still higher than the upper border level of 90 kcal/mol. All other H-BDE values are much higher than the desired values and indicate that these molecules are stable in open air and in the presence of oxygen. Concerning the BDE values of the rest of the single acyclic bonds it is also evident that BDE values for the abstraction of iodine atoms are significantly lower (6–7 kcal/mol) than the BDE values for the abstraction of bromine atoms.

Besides oxidation reactions, hydrolysis is also important mechanism for the degradation of organic materials. Stability of organic molecules in water by explicit inclusion of water molecules can be computationally investigated thanks to the MD

simulations. After MD simulations atoms with pronounced interactions with water can be determined by calculation of the radial distribution functions, which also has been done in this work, Fig.S3 (supporting information).

In cases of both newly synthetized quinoline derivatives hydrogen atoms (H18) of OH group have the most pronounced interactions with water molecules. RDFs of these atoms are characterized with the two distinct solvation spheres. The first maximal g(r) values for the RDF of H18 in both cases are located at distance of around 1.7 Å. Other atoms of both derivatives with significant interactions with water molecules are oxygen atoms (O10), bromine/iodine atoms, and carbon atoms C8 and C9. In general, interaction energies of DBHQ(**1)** and DIHQ(**2)** with water according to MD simulations are very similar, further indicating that both of these derivatives have very similar stability in water. However, both of these quinoline derivatives are having higher interaction energies with water than pristine quinoline, for which we calculated interaction energy in our previously submitted article [28].

4.4 Nonlinear optical properties

The calculated polarizability of DBHQ(**1)** and DIHQ(**2)** are 2.397×10^{-23} and 2.882×10^{-23} esu. The dipole moments of DBHQ(**1)** and DIHQ(**2)** are respectively, 3.5783 and 3.8456 Debye. The first order hyperpolarizabilities are 6.899×10^{-30} and 8.387×10^{-30} esu for DBHQ(**1)** and DIHQ(**2)** which are comparable with the reported values of similar derivatives [54] and these values are 53.07 and 64.52 times that of the standard NLO material urea [74]. The reported values of first hyperpolarizability of similar derivatives are 5.37×10^{-30} [54] and 16.9×10^{-30} esu [75]. The theoretically predicted second order hyperpolarizabilities are -8.062×10^{-37}esu for DBHQ(**1)** and -9.311×10^{-37}esu for DIHQ(**2)** and the reported values are -28.33×10^{-37} esu [54], -21.14×10^{-37} esu [76]. Hence the title compounds and its derivatives are good objects for further studies of nonlinear optical properties. In the title compounds, Br-Br and I-I atoms are replaced by Br-I substitution with Br near to OH and I away from OH and vice-versa. The polarizability values of title compounds slightly reduced during substitution with Br and I atoms. The first order hyperpolarizability value of I near to OH (IHQ(4)) is in agreement with DIHQ(2) whereas Br near to OH (BHQ(3)) is agreement with DBHQ(1). Second order

hyperpolarizability values of IHQ(4) and BHQ(3) lie in between those of the title compounds (table S1-supporting information).

4.5 Frontier molecular orbital analysis

Frontier molecular orbitals are investigated in order to understand global stability and reactive properties of the title compounds. Visualization presented in Fig. S4 (supporting information) indicates the importance of iodine and bromine atoms, as HOMO is practically completely delocalized in the near vicinity of these atoms. This result designates iodine and bromine atoms to act as electron donor during the interactions with other molecules. HOMO is delocalized over the entire region except H-atoms of DBHQ(**1)** and except for the ring PhII and H-atoms of DIHQ(**2)**. On the other side LUMO is mainly delocalized over the entire rings of the title molecules. For IHQ(4) and BHQ(3), LUMO is all over the molecule except Br atom; in the case BHQ(3), HOMO is delocalized except Br and H atoms while for IHQ(4), HOMO is all over the molecule except PhII and Br atom. Using information on the energies of HOMO and LUMO, useful and frequently used quantum-molecular descriptors such as the ionization energy and electron affinity can be calculated according to the following simple relations: $I = -E_{HOMO}$, $A = -E_{LUMO}$, $\eta = (-E_{HOMO} + E_{LUMO})/2$ and $\mu = (E_{HOMO} + E_{LUMO})/2$ [77]. Parr et al. [78] proposed the global electrophilicity power of a ligand as $\omega = \mu^2/2\eta$. For the title compounds, energy difference between HOMO and LUMO, HOMO-LUMO gap, are equal to 2.87 eV for DBHQ(**1)** and 0.78eV for DIHQ(**2)**. Ionization potential, I, and electron affinity, A, are calculated to be 8.14 eV, 5.27 eV and 5.88 eV, 5.10 eV for DBHQ(**1)** and DIHQ(**2)**, respectively. The values of HOMO-LUMO gap and global hardness (η = 1.44 eV for DBHQ(**1)** and 0.39 eV for DIHQ(**2**) are almost the same as in the case of other similar derivatives that we have previously investigated [54,76]. Although the stability parameters of these derivatives are practically the same, there are significant differences in the values of chemical potential and global electrophilicity. Also, the calculated electrophilicity of the DBHQ(**1)** and DIHQ(**2)** molecules are 15.63 eV and 38.64 eV, which is significantly lower than the value of electrophilicity of derivative in the work of Rajeev et al. [54,76], with the values of 28.29 and 24.40 eV, meaning that the title molecules are much more stable. IHQ(4) and BHQ(3) chemical descriptors are in agreement with DIHQ(2) values (table S1-supporting information).

4.6 Molecular electrostatic potential maps

Molecular electrostatic potential (MEP) simultaneously displays molecular shape, size and electrostatic potential in terms of colour grading. MEP map has been found to be a very helpful tool in the analysis of the correlation amide molecular structures with its physiochemical property relationship, including biomolecules and drugs [79]. It provides a visual technique to comprehend the relative polarity of the molecule as shown in Fig.S5 (supporting information). Different values of the electrostatic potential are represented by various colours; red<organge<yellow<green<blue. In the MEP maximum negative region represents the site for electrophilic attack indicated by red colour while the maximum positive region represents nucleophilic attack indicated by blue colour. From the MEP plot of the title compounds it is clearly seen that for DBHQ(1) O, Br atoms, phenyl ring are most electronegative region suitable for electrophilic attack and hydrogen atoms are most electropositive region suitable for nucleophilic attack while for DIHQ(2), iodine atoms are electro positive and rings and oxygen atom are electro negative. There is no change in electrophilic (Phenyl ring, Br, O atoms) and nucleophilic site (Iodine atom) for IHQ(4) and BHQ(3).

4.7 Natural Bond Orbital (NBO) Analysis

The natural bond orbitals (NBO) calculations were performed using NBO 3.1 program [80] as implemented in the Gaussian09 package at the DFT/B3LYP level and the important results are tabulated in tables 3 and 4. The strong interaction $n_2O_{11}\rightarrow\pi^*(C_3$-C2) has the highest E(2) value 37.87 kcal/mol and a very strong interaction has been in $n_1N7\rightarrow\sigma^*(C5\text{-}C_4)$ with an energy of 10.49 kcal/mol for DBHQ(**1)** and the strong interaction $n_1C5\rightarrow\pi^*$(C9-C10) has the highest E(2) value 59.36 kcal/mol and a very strong interaction has been in $n_1N7\rightarrow\sigma^*$(C9-C8) with an energy of 10.14 kcal/mol for DIHQ(**2)**. Almost 100% p-character was observed in π bonding of C1-C6, C3-C2 and the lone pairs of n_2O_{11}, n_3Br13 and n_3Br12 for DBHQ(**1)** and in π bonding of C6-C1, C3-C2 and the lone pairs of n_1C5, n_3I12 and n_3I13 for DIHQ(**2)**.

4.8 Molecular docking studies

Protozoal organisms are one of the leading agents of mortality in humans [81]. Two leading protozoal organisms viz.; Plasmodium falciparum and Entamoeba Histolytica

cause Malaria and amoebiasis respectively [82]. The major treatment method remains chemotherapy and there is a need to develop new molecules so as to cater the growing resistance to the drugs available in market [83]. PASS [84] gives the biological activity spectrum of a compound and predicts the title ligands to be Antiprotozoal (Amoeba) agents with P_a score of 0.96 and 0.91 (table 4). To further establish their antiprotozoal activity, we decided to carry out molecular docking studies of the compound against Plasmodium falciparum dihydrofolatereductase-thymidylate synthase (PfDHFR-TS) [PDB ID: 3QGT]. The PDB structure 3QGT [85] was selected for docking as the reported structure has been established from X-ray Crystallographic data with a good resolution of 2.3 Å. Further the enzyme has an attached co-crystallized inhibitor so has a well defined binding site which could be targeted. Molecular docking has recently been used as a convenient tool to get insights into the molecular mechanism of protein ligand interactions [86]. All docking calculations were performed on AutoDock-Vina software [87]. The docking protocol was tested by docking the co-crystallized inhibitor onto the enzyme catalytic site which showed perfect synergy with the co crystallized ligand with RMSD close to zero (Fig.S6-supporting information). Amongst the docked conformations the best scored conformation predicted by AutoDock scoring function was visualized in DSV, LigPlot and Pymol software for ligand–protein interactions. The molecule binds at the catalytic site of the substrate by weak non-covalent interactions (Fig.6). Amino acid Ile164 forms hydrogen bond with the oxygen atom of hydroxy group attached to ligand DIHQ(2) (Fig.S7(a)-supporting information). Phe58 forms π- π interaction with benzene ring of the ligand (Fig.S7 (b)). DBHQ(1) forms one H-bond with NDP and one with Ile164 in addition to π- π interaction with Phe58 (Fig.S7(c,d). Amino acids Phe58 Asp54 Ile112 Ile164 and NDP surround the ligand molecules and hold it by non-covalent and hydrophobic interactions. Docking scores of -6.7 and -6.3 kcal/mol for DBHQ(1) and DIHQ(2) respectively. For BHQ(3), the residues of the amino acids Phe136 forms halogen and π-alkyl interaction with bromine atom attached to the phenyl ring while Leu106 shows π-sigma interaction with phenyl ring. Leu250, Ile170 shows alkyl interactions with Iodine, bromine atom attached with phenyl ring respectively and for IHQ(4) the amino acids of the receptors Leu106 forms π-alkyl and π-sigma interaction with title compound while Phe136 gives H-bond with CH bond of the

phenyl ring; Leu250, Tyr373 alkyl interactions with iodine, bromine atoms of the phenyl ring. Binding affinity value of BHQ(3) and IHQ(4) are that of DIHQ(2) . These results reveal that the ligands bind at the active site of the macromolecule and could restrict or block the functioning of Plasmodium falciparum dihydrofolatereductase-thymidylate synthase (PfDHFR-TS), there by acting as antiprotozoal agents.

5. Conclusions

By combining the experimental and theoretical information, complete vibrational analysis of the title compounds are performed. The nonlinear optical properties are also predicted theoretically and the calculated NLO properties of the title compounds are greater than that of urea and therefore the title compounds are good objects for further studies in nonlinear optics. The molecular calculations like natural bond orbitals, HOMO-LUMO and molecular electrostatic potential surface were also performed. ALIE surfaces indicate that introduced bromine and iodine atoms are the molecule sites with the lowest ALIE values and therefore the molecule sites that are prone to electrophilic attacks. It is interesting that the lowest ALIE value in the case of derivative with iodine atoms (DIHQ(**2)**) is practically the same as the lowest ALIE value of pristine quinoline. Derivative DIHQ(**2)** is characterized by four intra-molecular noncovalent interactions, among which the strongest are the ones including iodine and the adjacent carbon atoms. Fukui functions indicate rather similar situation for both derivatives, showing that the possibly important reactive sites could be carbon atoms C5, C8 and C10. H-BDE values indicate that the investigated derivatives are stable towards the autoxidation mechanism, while RDFs indicate that the hydrogen atom H18 of the OH group is having the most pronounced interactions with water molecules. Molecular docking studies suggest that the title compounds could restrict or block the functioning of Plasmodium falciparum dihydrofolatereductase-thymidylate synthase (PfDHFR-TS), there by acting as antiprotozoal agents. Halogens substituent effects of NLO, MEP, frontier molecular orbital analysis and docking studies are also reported and halogenations are in significant advance for improving the ligand bioefficiency.

Acknowledgments

Part of this work has been performed thanks to the support received from Schrödinger Inc. Part of this study was conducted within the

project funded by the Ministry of Education, Science and Technological Development of Serbia, grant number III41017.

References

[1] M. Kidwai, K.R. Bhushan, P. Sapra, R.K. Saxena, R. Gupta, Alumina-supported of antibacterial quinolines using microwaves, Bioorg. Med. Chem. 8(1) (2000) 69-72.

[2] S. Tewari, P.M.S. Chauhan, A.P. Bhaduri, N. Fatima, R.K. Chatterjee, Syntheses and antifilarial profile of 7-chloro-4-(substituted amino) quinolines, a new class of antifilarial agents, Bioorg. Med. Chem. Lett. 10 (2000) 1409-1412.

[3] T. Narender, S.K. Tanvir, M.S. Rao, K. Srivastava, S.K. Puri, Prenylatedchalcones isolated from Ctotalaria genus inhibits in vitro growth of the human malaria parasite Plasmodium falciparum, Bioorg. Med. Chem. Lett. 15 (2005) 2453-2455.

[4] R.F. Hector, An overview of antifungal drugs and their use for treatment of deep and superficial mycoses in animals, Clin. Tech. Small Anim. Pract. 20 (2005) 240-249.

[5] K.M. Khan, Z.S. Saify, Z.A. Khan, M. Ahmed, M. Saeed, M. Schick, H.J. Kohlbau, W. Voelter, Antibiotics, Antiviral drugs, chemotherapeutics. cytostatics-syntheses and cytotoxic antimicrobial, antifungal and cardiovascular activity of new quinoline derivatives, Arzheim. Forsch-Drug Res. 50 (2000) 915-924.

[6] A. Nayyar, A. Malde, E. Coutinho, R. Jain, Synthesis, anti-tuberculosis activity and 3D-QSAR study of ring-substituted-2/4-quinolinecarbaldehyde derivatives, Bioorg. Med. Chem. 14 (2006) 7302-7310.

[7] Y. Kuroda, M. Ogawa, H. Nasu, M. Jerashima, M. Kasahara, Y. Kiyama, M. Wakita, Y. Fujiwara, N. Fujii, J. Nakagawa, Locations of local anesthetic dibucaine in model membranes and the interaction between dibucaine and a Na+ channel inactivation gate peptide as studied by 2H- and 1H-NMR spectroscopies, Biophys. J. 71 (1996) 1191-1207.

[8] L.W. Deady, J. Desneves, A.J. Kaye, G.J. Finlay, B.C. Baguley, W.A. Denny, Positioning of the carboxamide side chain11-oxo-11H-indeno[1,2-

b]quinolinecarboxamide anticancer agents, effects on cytotoxicity, Bioorg. Med. Chem. 9 (2001) 445-452.

[9] M.L. Martinez, W.C. Cooper, P.-T. Chou, A novel excited-state intramolecular proton transfer molecule, 10-hydroxybenzo [h] quinoline, Chem. Phys. Lett. 193 (1992) 151-154.

[10] S. Takeuchi, T. Tahara, Coherent Nuclear Wavepacket Motions in Ultrafast Excited-State Intramolecular Proton Transfer: Sub-30-fs Resolved Pump− Probe Absorption Spectroscopy of 10-Hydroxybenzo [h] quinoline in Solution, J. Phys. Chem. 109A (2005) 10199-10207.

[11] H. Matsumiya, H. Hoshino, T. Yotsuyanagi, A novel fluorescence reagent, 10-hydroxybenzo [h] quinoline-7-sulfonate, for selective determination of beryllium (II) ion at pg cm− 3 levels, Analyst, 126 (2001) 2082-2086.

[12] R.T. Ulahannan, C.Y. Panicker, H.T. Varghese, C. Van Alsenoy, R. Musiol, J. Jampilek, P.L. Anto, Vibrational spectroscopic, 1H NMR and quantum chemical computational study of 4-hydroxy-2-oxo-1, 2-dihydroquinoline-8-carboxylic acid, Spectrochim. Acta 121 (2014) 445-456.

[13] Z. He, G. Milburn, K. Baldwin, D. Smith, A. Danel, P. Tomasik, The efficient blue photoluminescence of pyrazolo-[3, 4-b]-quinoline derivatives and the energy transfer in polymer matrices, J. Luminesc. 86 (2000) 1-14.

[14] J. Niziol, A. Danel, G. Boiteux, J. Davenas, B. Jarosz, A. Wisla, G. Seytre, Optical properties of new pyrazolo [3, 4-b] quinoline and its composites, Syn. Met. 127 (2002) 175-180.

[15] A.J. Epstein, Electrically conducting polymers, science and technology, Mater. Res. Soc. Bull. 22 (1997) 16-24.

[16] S. Schettigar, K. Chandrasekharan, G. Umesh, B.K. Sarojini, B. Narayana, Studies on nonlinear optical parameters of bis-chalcone derivatives doped polymer, Polymer 47 (2006) 3565-3567.

[17] B. Dekavaux-Nicot, J. Maynadie, D. Lavabre, S. Fery-Forgues, Ca^{2+}vs Ba^{2+} electrochemical detection by two disubstituted ferrocenylchalcone chemosensors, study of the ligand metal interactions in CH^3CN, J. Organomet. Chem. 692 (2007) 874-886.

[18] A. Lakshmi, V. Balachandran, A. Janaki, Comparative vibrational spectroscopic studies, HOMO-LUMO and NBO analysis of 5,7-dibromono-8-hydroxyquinoline and 5,7-dichloro-8-hydroxyquinoline based on Density Functional Theory, J. Mo. Struct. 1004 (2011) 51-66.

[19] P. Lienard, J. Gavartin, G. Boccardi, M. Meunier, Predicting drug substances autoxidation, Pharm. Res. 32(1) 2015) 300-310.

[20] G.L. de Souza, L.M. de Oliveira, R.G. Vicari, A. Brown, A DFT investigation on the structural and antioxidant properties of new isolated interglycosidic O-(1→ 3) linkage flavonols, J. Mol. Model. 22(4) (2016) 1-9.

[21] Z. Sroka, B. Żbikowska, J. Hładyszowski, The antiradical activity of some selected flavones and flavonols, Experimental and quantum mechanical study, J. Mol. Model. 21(12) (2015) 1-11.

[22] S. Armaković, S.J. Armaković, S. Koziel, Optoelectronic properties of curved carbon systems, Carbon, 111 (2017) 371-379.

[23] S. Armaković, S. J. Armaković, J. P. Šetrajčić, I.J. Šetrajčić, Active components of frequently used β-blockers from the aspect of computational study, J. Mol. Model. 18(9) (2012) 4491-4501.

[24] S.J. Armaković, S. Armaković, N.L. Finčur, F. Šibul, D. Vione, J.P. Šetrajčić, B. Abramović, Influence of electron acceptors on the kinetics of metoprolol photocatalytic degradation in TiO 2 suspension. A combined experimental and theoretical study, RSC Adv. 5(67) (2015) 54589-54604.

[25] M. Blessy, R.D. Patel, P.N. Prajapati, Y. Agrawal, Development of forced degradation and stability indicating studies of drugs-A review, J. Pharm. Anal. 4(3) (2014) 159-165.

[26] B. Abramović, S. Kler, D. Šojić, M. Laušević, T. Radović, D. Vione, Photocatalytic degradation of metoprolol tartrate in suspensions of two TiO 2-based photocatalysts with different surface area. Identification of intermediates and proposal of degradation pathways, J. Hazard. Mater. 198 (2011) 123-132.

[27] S.J. Armaković, M. Grujić-Brojčin, M. Šćepanović, S. Armaković, A. Golubović, B. Babić, B.F. Abramović, Efficiency of La-doped TiO_2 calcined at different

temperatures in photocatalytic degradation of β-blockers, Arab. J. Chem. doi.org/10.1016/j.arabjc.2017.01.001.

[28] B. Sureshkumar, Y.S. Mary, C.Y. Panicker, S. Suma, S. Armaković, S.J. Armaković, C. Van Alsenoy, B. Narayana, Quinoline derivatives as possible lead compounds for anti-malarial drugs: Spectroscopic, DFT and MD study, Arab. J. Chem. doi.org/10.1016/j.arabjc.2017.07.006.

[29] S. Armaković, S.J. Armaković, B.F. Abramović, Theoretical investigation of loratadine reactivity in order to understand its degradation properties: DFT and MD study, J. Mol. Model. doi.org/10.1007/s00894-016-3101-2.

[30] S.J. Armaković, S. Armaković, D.D. Četojević-Simin, F. Šibul, B.F. Abramović, Photocatalytic degradation of 4-amino-6-chlorobenzene-1,3-disulfonamide stable hydrolysis product of hydrochlorothiazide: detection of intermediates and their toxicity, Environmental Pollution, 233 (2018) 916-924.

[31] D.D. Četojević-Simin, S.J. Armaković, D.V. Šojić, B.F. Abramović, Toxicity assessment of metoprolol and its photodegradation mixtures obtained by using different type of TiO 2 catalysts in the mammalian cell lines, Sci. Total Environ. 463 (2013) 968-974.

[32] Gaussian 09, Revision B.01, M. J. Frisch, G. W. Trucks, H. B. Schlegel, G. E. Scuseria,M. A. Robb, J. R. Cheeseman, G. Scalmani, V. Barone, B. Mennucci, G. A. Petersson, H. Nakatsuji, M. Caricato, X. Li, H. P. Hratchian, A. F. Izmaylov, J. Bloino, G. Zheng, J. L. Sonnenberg, M. Hada, M. Ehara, K. Toyota, R. Fukuda, J. Hasegawa, M. Ishida, T. Nakajima, Y. Honda, O. Kitao, H. Nakai, T. Vreven, J. A. Montgomery, Jr., J. E. Peralta, F. Ogliaro, M. Bearpark, J. J. Heyd, E. Brothers, K. N. Kudin, V. N. Staroverov, T. Keith, R. Kobayashi, J. Normand, K. Raghavachari, A. Rendell, J. C. Burant, S. S. Iyengar, J. Tomasi, M. Cossi, N. Rega, J. M. Millam, M. Klene, J. E. Knox, J. B. Cross, V. Bakken, C. Adamo, J. Jaramillo, R. Gomperts, R. E. Stratmann, O. Yazyev, A. J. Austin, R. Cammi, C. Pomelli, J. W. Ochterski, R. L. Martin, K. Morokuma, V. G. Zakrzewski, G. A. Voth, P. Salvador, J. J. Dannenberg, S. Dapprich, A. D. Daniels, O. Farkas, J. B. Foresman, J. V. Ortiz, J. Cioslowski, D. J. Fox, Gaussian, Inc., Wallingford CT, 2010.

[33] J.B. Foresman, in: E. Frisch (Ed.), Exploring Chemistry with Electronic Structure Methods: a Guide to Using Gaussian, 1996, Pittsburg, PA.

[34] R. Dennington, T. Keith, J. Millam, GaussView, Version 5, Semichem Inc., Shawnee Mission KS, 2009.

[35] J.M.L. Martin, C. Van Alsenoy, GAR2PED, a Program to Obtain a Potential Energy Distribution from a Gaussian Archive Record, University of Antwerp, Belgium, 2007.

[36] A.D. Bochevarov, E. Harder, T.F. Hughes, J.R. Greenwood, D.A. Braden, D.M. Philipp, D. Rinaldo, M.D. Halls, J. Zhang, R.A. Friesner, Jaguar: A high performance quantum chemistry software program with strengths in life and materials sciences, Int. J. Quantum Chem. 113(18) (2013) 2110-2142.

[37] D. Shivakumar, J. Williams, Y. Wu, W. Damm, J. Shelley, W. Sherman, Prediction of absolute solvation free energies using molecular dynamics free energy perturbation and the OPLS force field, J. Chem. Theor. Comput. 6(5) (2010) 1509-1519.

[38] Z. Guo, U. Mohanty, J. Noehre, T.K. Sawyer, W. Sherman, G. Krilov, Probing the α-Helical Structural Stability of Stapled p53 Peptides: Molecular Dynamics Simulations and Analysis, Chem. Biol. Drug Design, 75(4) (2010) 348-359.

[39] K.J. Bowers, E. Chow, H. Xu, R.O. Dror, M.P. Eastwood, B.A. Gregersen, J.L. Klepeis, I. Kolossvary, M.A. Moraes, F.D. Sacerdoti. Scalable algorithms for molecular dynamics simulations on commodity clusters. in SC 2006 Conference, Proceedings of the ACM/IEEE. 2006. IEEE.

[40] V.B. Bregović, N. Basarić, K. Mlinarić-Majerski, Anion binding with urea and thiourea derivatives, Coord. Chem. Rev. 295 (2015) 80-124.

[41] A.D. Becke, Densityfunctional thermochemistry. III. The role of exact exchange, J. Chem. Phys. 98(7) (1993) 5648-5652.

[42] E. Harder, W. Damm, J. Maple, C. Wu, M. Reboul, J.Y. Xiang, L. Wang, D. Lupyan, M.K. Dahlgren, J.L. Knight, OPLS3: a force field providing broad coverage of drug-like small molecules and proteins, J. Chem. Theor. Comput. 12(1) (2015) 281-296.

[43] W.L. Jorgensen, D.S. Maxwell, J. Tirado-Rives, Development and testing of the OPLS all-atom force field on conformational energetics and properties of organic liquids. J. Am. Chem. Soc. 118(45) (1996) 11225-11236.

[44] W.L. Jorgensen, J. Tirado-Rives, The OPLS [optimized potentials for liquid simulations] potential functions for proteins, energy minimizations for crystals of cyclic peptides and crambin. J. Am. Chem. Soc. 110(6) (1988) 1657-1666.

[45] H.J. Berendsen, J.P. Postman, W.F. van Gunsteren, J. Hermans, Interaction models for water in relation to protein hydration, in Intermolecular forces. 1981, Springer. p. 331-342.

[46] A. Otero-de-la-Roza, E.R. Johnson, J. Contreras-García, Revealing non-covalent interactions in solids: NCI plots revisited, Phys. Chem. Chem. Phys. 14(35) (2012) 12165-12172.

[47] E.R. Johnson, S. Keinan, P. Mori-Sanchez, J. Contreras-Garcia, A.J. Cohen, W. Yang, Revealing noncovalent interactions, J. Am. Chem. Soc. 132(18) (2010) 6498-6506.

[48] Schrödinger Release 2017-3: Maestro, Schrödinger, LLC, New York, NY, 2017

[49] G. Varsanyi, Assignments for Vibrational Spectra of Seven Hundred Benzene Derivatives, Wiley, New York, 1974.

[50] Y.S. Mary, C.Y. Panicker, P.L. Anto, M. Sapnakumari, B. Narayana, B.K. Sarojini, Molecular structure, FT-IR, NBO, HOMO and LUMO, MEP and first order hyperpolarizability of (2E)-1-(2,4-dichlorophenyl)-3-(3,4,5-trimethoxyphenyl)prop-2-en-1-one by HF and density functional methods, Spectrochim. Acta 135 (2015) 81-92.

[51] N.P.G. Roeges, A Guide to the Complete Interpretation of Infrared Spectra of Organic Structures, John Wiley and Sons., New York, 1994.

[52] C.Y. Panicker, H.T. Varghese, D. Philip, H.I.S. Nogueira, K. Castkova, Raman, IR and SERS spectra of methyl(2-methyl-4,6-dinitrophenylsulfanyl)ethanoate, Spectrochim. Acta 67 (2007) 1313-1320.

[53] G. Socrates, Infrared and Raman Characteristic Group Frequencies, Wiley, Middlesex, UK, 2001.

[54] R.T. Ulahannan, C.Y. Panicker, H.T. Varghese, R. Musiol, J. Josef, C. Van Alsenoy, J.A. War, S.K. Srivastava, Molecular Structure, FT-IR, FT-Raman, NBO, HOMO and LUMO, MEP, NLO and molecular docking study of 2-[(E)-2-(2-bromophenyl)-ethenyl]quinoline-6-carboxylic acid, Spectrochim. Acta 151 (2015) 184-197.

[55] N.B. Colthup, L.H. Daly, S.E. Wiberly, Introduction to Infrared and Raman Spectroscopy, Academic Press, New York, 1990.

[56] R.M. Silverstein, G.C. Bassler, T.C. Morril, Spectrometric Identification of Organic Compounds, fifth ed., John Wiley and Sons Inc., Singapore, 1991.

[57] S. Arshad, R.R. Pillai, D.A. Zainuri, N.C. Khalib, I.A. Razak, S. Armakovic, S.J. Armakovic, R. Renjith, C.Y. Panicker, C. Van Alsenoy, Synthesis, XRD crystal structure, spectroscopic characterization, local reactive properties using DFT and molecular dynamics simulations and molecular docking study of (E)-1-(4-bromophenyl)-3-(4-trifluoromethoxy)phenyl)prop-2-en-1-one, J. Mol. Struct. 1137 (2017) 419-430.

[58] D.A. Zainuri, S. Arshad, N.C. Khalib, I.A. Razak, R.R. Pillai, S.F. Sulaiman, N.S. Hashim, K.L. Ooi, S. Armakovic, S.J. Armakovic, C.Y. Panicker, C. Van Alsenoy, Synthesis, XRD crystal Structure, spectroscopic characterization (FT-IR, ^{1}H and ^{13}C NMR), DFT studies, chemical reactivity and bond dissociation energy studies using molecular dynamics simulations and evaluation of antimicrobial and antioxidant activities of a novel chlacone derivative, (E)-1-(4-bromophenyl)-3-(4-iodophenyl)prop-2-en-1-one, J. Mol. Struct. 1128 (2017) 520-533.

[59] J.S. Murray, J.M. Seminario, P. Politzer, P. Sjoberg, Average local ionization energies computed on the surfaces of some strained molecules, Int. J. Quantum Chem. 38(S24) (1990) 645-653.

[60] P. Politzer, F. AbuAwwad, J.S. Murray, Comparison of density functional and Hartree–Fock average local ionization energies on molecular surfaces, Int. J. Quantum chem. 69(4) (1998) 607-613.

[61] F.A. Bulat, A. Toro-Labbé, T. Brinck, J.S. Murray, P. Politzer, Quantitative analysis of molecular surfaces: areas, volumes, electrostatic potentials and average local ionization energies, J. Mol. Model. 16(11) (2010) 1679-1691.

[62] P. Politzer, J.S. Murray, F.A. Bulat, Average local ionization energy: a review, J. Mol. Model. 16(11) (2010) 1731-1742.

[63] A. Michalak, F. De Proft, P. Geerlings, R. Nalewajski, Fukui functions from the relaxed Kohn-Sham orbitals, J. Phys. Chem. A, 103(6) (1999) 762-771.

[64] X. Ren, Y. Sun, X. Fu, L. Zhu, Z. Cui, DFT comparison of the OH-initiated degradation mechanisms for five chlorophenoxy herbicides, J. Mol. Model. 19(6) (2013) 2249-2263.

[65] L.-l. Ai, J.-y. Liu, Mechanism of OH-initiated atmospheric oxidation of E/Z-CF3CF=CFCF3: a quantum mechanical study, J. Mol. Model. 20(4) (2014) 1-10.

[66] W. Sang-aroon, V. Amornkitbamrung, V. Ruangpornvisuti, A density functional theory study on peptide bond cleavage at aspartic residues: direct vs cyclic intermediate hydrolysis, J. Mol. Model. 19(12) (2013) 5501-5513.

[67] J. Kieffer, É. Brémond, P. Lienard, G. Boccardi, In silico assessment of drug substances chemical stability, J. Mol. Struct. THEOCHEM, 954(1) (2010) 75-79.

[68] S.W. Hovorka, C. Schöneich, Oxidative degradation of pharmaceuticals: theory, mechanisms and inhibition, J. Pharm. Sci. 90(3) (2001) 253-269.

[69] K.A. Connors, G.L. Amidon, V.J. Stella, Chemical stability of pharmaceuticals: a handbook for pharmacists, 1986: John Wiley & Sons.

[70] D. Johnson, L. Gu, Autoxidation and antioxidants, Encycl. Pharma. Technol. 1 (1988) 415-449.

[71] J.S. Wright, H. Shadnia, L.L. Chepelev, Stability of carbon□centered radicals: Effect of functional groups on the energetics of addition of molecular oxygen, J. Comput. Chem. 30(7) (2009) 1016-1026.

[72] G. Gryn'ova, J.L. Hodgson, M.L. Coote, Revising the mechanism of polymer autoxidation, Org. Biomol. Chem. 9(2) (2011) 480-490.

[73] T. Andersson, A. Broo, E. Evertsson, Prediction of Drug Candidates' Sensitivity Toward Autoxidation: Computational Estimation of C-H Dissociation Energies of Carbon-Centered Radicals, J. Pharm. Sci. 103(7) (2014) 1949-1955.

[74] C. Adant, M. Dupuis, J.L. Bredas, Ab initio study of the nonlinear optical properties of urea, electron correlation and dispersion effects, Int.J. Quantum Chem. 56 (2004) 497-507.

[75] R.T. Ulahannan, C.Y. Panicker, H.T. Varghese, R. Musiol, J. Josef, C. Van Alsenoy, J.A. War, A.A. Al-Saadi, Vibrational spectroscopic and molecular docking study of (2E)-N-(4-chloro-2-oxo-1,2-dihydroquinoline-3-yl]-3-phenylprop-2-enamide, Spectrochim. Acta 151 (2015) 335-349.

[76] R.T. Ulahannan, C.Y. Panicker, H.T. Varghese, R. Musiol, J. Josef, C. Van Alsenoy, J.A.War, T.K. Manojkumar, Vibrational spectroscopic and molecular docking study of 2-[(E)-2-phenylethenyl]quinoline-5-carboxylic acid, Spectrochim. Acta 150 (2015) 190-199.

[77] K. Fukui, Role of frontier orbitals in chemical reactions, Science 218 (1982) 747-754.

[78] R.G. Parr, R.G. Pearson, Absolute hardness: companion parameter to absolute electronegativity, J. Am. Chem. Soc. 105 (1983) 7512-7516.

[79] J.A. War, K. Jalaja, Y.S. Mary, C.Y. Panicker, S. Armakovic, S.J. Armakovic, S.K. Srivastava, C. Van Alsenoy, Spectroscopic characterization of 1-[3-(1*H*-imidazol-1-yl)propyl]-3-phenylthiourea and assessment of reactive and optoelectronic properties employing DFT calculations and molecular dynamics simulations, J. Mol. Struct. 1129 (2017) 72-85.

[80] E.D. Glendening, A.E. Reed, J.E. Carpenter, F. Weinhold, NBO Version 3.1, Gaussian Inc., Pittsburgh, PA, 2003.

[81] World Health Organization, status 2014, http://www.who.int/malaria/media/world malaria report 2013/en/.

[82] W.E. Collins, GM.Jeffery, Plasmodium malariae, parasite and disease, Clin. Microbiol. Rev. 20 (2007) 579-592.

[83] S. Becker, P. Hoffman, E. R. Houpt, Efficacy of antiamebic drugs in a mouse model, Am. J. Trop. Med. Hyg., 84 (2011) 581-586.

[84] A. Lagunin, A. Stepanchikova, D. Filimonov, V. Poroikov, PASS: prediction of activity spectra for biologically active substances, Bioinformatics 16 (2000) 747-748.

[85] J. Vanichtanakul, S. Taweechai, J. Yuganiyama, T. Vilaivan, P. Chitnumsub, S. Kamchonwonqpaisan, Y. Yuthavong, Trypanosomaldihydrofolatereductase reveals natural antifolate resistance, ACS Chem. Biol. 6(9) (2011) 905-911.

[86] J.A. War, S.K. Srivastava, S.D. Srivastava, Synthesis and DNA binding study of imidazole linked thiazolidinone derivatives, Luminescence, 32(1) (2017) 104-113.

[87] O. Trott, A. J. Olson, AutoDockVina: Improving the speed and accuracy of docking with a new scoring function, efficient optimization and multithreading, J. Comput. Chem. 31 (2010) 455-461.

Figure captions

Fig.1 Optimized geometries of DBHQ(**1**) and DIHQ(**2**)

Fig.2 ALIE surfaces of DBHQ(**1**) and DIHQ(**2**)

Fig.3 Intramolecular noncovalent interactions of DBHQ(**1**) and DIHQ(**2**) with corresponding strengths expressed in terms of electron density (electron/bohr^3)

Fig.4 Fukui functions a) f^+ and b) f^- of the DBHQ(**1**) and DIHQ(**2**)

Fig.5 BDEs of all single acyclic bonds of DBHQ(**1**) and DIHQ(**2**). (H-BDEs are provided in red, while the rest of BDE values are provided in blue color)

Fig.6 (A) Both DBHQ(**1**) and DIHQ(**2**), (B) BHQ(3) and (C) IHQ(4) bind at the active site of PfDHFR

Table 1

Calculated scaled wavenumbers, observed IR, Raman bands and vibrational assignments of the title compounds

DBHQ(**1**)

B3LYP/SDD			IR	Raman	Assignments[a]
υ(cm^{-1})	IR_I	R_A	υ(cm^{-1})	υ(cm^{-1})	-
3457	103.46	64.39	3440	3455	υOH(100)
3090	0.90	52.54	-	-	υCHI(99)
3083	6.71	146.91	-	3085	υCHII(98)
3067	9.59	143.01	3070	3070	υCHII(94)
3037	19.83	157.05	-	3040	υCHII(99)
1585	19.01	48.45	1583	1584	υPhI(41)
1568	18.43	2.72	1570	1566	υPhII(50), υPhI(14), δCHII(11)
1537	15.48	77.31	-	1540	υPhII(34), υPhI(42)
1461	79.70	18.76	1459	1460	υPhI(45),υPhII(18)
1428	93.60	1.75	-	1430	δCHII(12), υPhI(15), υPhII(43)
1381	147.07	120.93	1388	1384	δOH(32), υPhI(19)
1363	25.33	24.75	1365	1365	δCHI(17), δCHII(19), υPhI(44)
1346	11.28	10.13	-	1344	υPhII(44), υPhI(26), δCHII(20)
1313	166.56	144.60	1320	1315	υPhI(37), δOH(15), υPhII(32)
1243	40.24	15.55	1244	1244	δCHII(48),υPhII(18)
1215	18.75	14.39	1210	1213	δCHI(49),υPhI(22), υPhII(10)
1181	96.26	11.33	-	-	υCO(33), υPhI(25)
1175	2.45	1.06	-	1177	υPhI(18), δCHII(47)
1115	17.02	11.21	1125	1125	δCHII(49), υPhII(14), υPhI(16)
1064	12.98	2.23	1050	-	υCO(13), δCHII(12), υPhII(15)
1021	6.37	21.85	-	1022	υPhI(62)
953	0.21	0.86	-	955	γCHII(89)
925	0.01	0.14	930	925	γCHII(92)
902	49.03	1.04	-	899	υPhII(62), δPhI(10), δPhII(12)
855	14.11	0.19	857	860	γCHI(86)

839	18.08	0.65	-	-	δPhII(35), υPhI(12)
780	28.52	0.23	784	782	γCHII(76), τPhII(11)
761	11.01	0.19	760	-	τPhI(33), τPhII(32), γCO(15)
703	19.87	34.00	695	696	δPhI(22), δPhII(20)
658	28.02	0.61	655	-	δPhI(17), υCBr(41), δPhII(21)
646	12.03	0.55	-	648	γCO(12), τPhII(11), τPhI(17), υCBr(38)
601	104.78	0.84	-	-	τOH(92)
596	11.53	0.64	593	595	δPhII(52), δCO(17)
574	1.58	0.12	-	570	τPhI(39), γCBr(23), τPhII(18)
547	13.45	5.53	555	-	δPhII(40), τPhI(16)
485	0.61	5.14	-	488	δPhI(59), δPhII(16)
482	0.05	0.03	-	-	τPhI(26), γCBr(22), τPhII(31)
417	0.85	1.03	-	420	τPhII(63), τPhI(10)
333	0.08	0.02	-	334	γCBr(29), γCO(16), τPhII(19), τPhI(10)
306	6.14	7.35	-	-	δCO(43)
282	1.26	2.45	-	285	δPhI(46), υCBr(16)
236	1.92	5.03	-	-	υCBr(17), δPhI(17), δCO(13)
226	1.12	0.19	-	224	τPhII(62), τPhI(14)
165	1.36	2.50	-	162	δCBr(65)
144	0.25	0.59	-	146	τPhI(54), τPhII(27)
121	0.01	2.18	-	-	δCBr(88)
109	0.07	2.27	-	111	γCBr(60), τPhII(19)
67	1.09	1.90	-	-	τPhI(72), τPhII(13)

[a]PhI-C1-C2-C3-C4-C5-C6; PhII-C4-C5-C10-C9-C8-N7;υ-stretching;δ-in-plane deformation ;γ-out-of-plane deformation; τ-torsion.

DIHQ(**2**)

B3LYP/SDD			IR	Raman	Assignments[a]
$\upsilon(cm^{-1})$	IR_I	R_A	$\upsilon(cm^{-1})$	$\upsilon(cm^{-1})$	-
3458	120.28	74.50	3426	3490	υOH(100)
3123	1.30	64.78	-	-	υCHI(97)

3122	18.85	214.13	-	3130	υCHII(97)
3100	6.15	67.56	-	3105	υCHII(100)
3088	10.30	98.15	3070	3067	υCHII(99)
1587	13.70	65.42	1590	1590	υPhI(42), υPhII(14)
1560	24.96	1.47	1558	1559	υPhII(50), υPhI(11), δCHII(13)
1528	21.14	86.60	1531	-	υPhI(46), υPhII(26)
1454	78.34	14.01	1453	1453	δCHII(20), υPhII(21),υPhI(46)
1420	53.87	2.64	-	-	υPhII(41),υPhI(42)
1380	46.03	293.45	1384	1381	δOH(39), υPhI(19), υPhII(14)
1361	18.25	15.77	1364	1361	δCHII(15), δCHI(24), υPhII(40)
1348	51.26	26.29	1340	1342	υPhI(47), δCHII(13), υPhII(15)
1301	188.06	22.97	-	1305	δOH(17),υPhI(14), υPhII(17)
1239	31.05	10.53	1241	1242	υPhII(48), δCHI(14), δCHII(17)
1222	26.81	25.22	1227	1226	υPhI(16), υPhII(11), δCHII(49)
1186	109.76	4.39	1189	1185	υCO(39), δCHI(36)
1162	81.74	8.93	-	1159	δCHII(55), δOH(18), υPhI(16)
1117	48.44	14.21	1110	1120	υPhI(20), υPhII(23), δCHII(40)
1057	12.94	2.37	1049	1049	δPhII(28), υCO(16), υPhII(13)
1018	8.06	27.08	1017	-	υPhI(59), δPhII(10)
999	0.50	0.87	988	996	γCHII(87), τPhII(10)
951	0.40	0.09	949	-	γCHII(88)
900	10.94	4.31	903	-	γCHI(85)
879	44.02	7.16	875	874	υPhII(52), δPhII(18), δPhI(17)
833	36.46	1.58	838	840	γCHII(54), τPhII(16), τPhI(11)
824	21.21	4.88	815	815	δPhI(28), δPhII(23)
796	19.99	0.48	792	793	τPhI (28), γCHII(25), τPhII (19)
693	17.57	43.85	691	-	δPhI(19), δPhII(18)
668	138.13	3.79	670	-	γCO(24), τPhI(17), τPhII(17)
662	35.33	1.37	-	658	τOH(42), τPhII(18), τPhI(13)
620	22.79	0.55	-	618	δPhI(33), δPhII(23)

600	0.22	3.92	604	-	γCI(20), τPhI(14), τPhII(21), γCO(12)
588	10.78	2.66	590	587	δPhII(56), δCO(14)
530	22.22	4.75	543	-	δPhII(27), δCI(24), δCO(11)
493	1.99	2.17	494	493	τPhII(33), τPhI(34), γCI(18)
485	0.78	3.53	-	480	δPhI(61), δPhII(13)
431	3.44	4.09	-	-	τPhII(65), τPhI(10)
334	0.16	2.77	-	336	γCI(45), γCO(19),τPhII(18)
282	9.94	5.44	-	286	υCI(42),δCO(19)
248	0.99	3.01	-	247	δPhI(16), υCI(42)
227	1.27	0.70	-	219	τPhII(65), γCI(10)
189	0.40	6.89	-	185	υCI(12)
148	0.20	0.69	-	-	τPhI(55), τPhII(31)
141	1.31	4.20	-	139	δCI(64), υCI(16)
98	0.44	1.28	-	-	γCI(60), τPhII(11)
88	0.08	4.30	-	85	δCI(87)
64	1.94	2.02	-	-	τPhI(69), τPhII(14)

[a]PhI-C1-C2-C3-C4-C5-C6; PhII-C4-C5-C10-C9-C8-N7;υ-stretching;δ-in-plane deformation ;γ-out-of-plane deformation; τ-torsion.

Table 2

Second-order perturbation theory analysis of Fock matrix in NBO basis corresponding to the intra molecular bonds of the title compounds

DBHQ(**1**)

Donor(i)	Type	ED/e	Acceptor(j)	Type	ED/e	E(2)[a]	E(j)-E(i)[b]	F(i,j)[c]
C1-C6	π	1.771	C5-C4	π*	0.472	16.60	0.29	0.067
-	-	-	C3-C2	π*	0.037	12.93	0.29	0.057
C1-C2	σ	1.971	C1-C6	σ*	0.022	3.38	1.31	0.059
-	-	-	C6-Br12	σ*	0.034	4.47	0.80	0.053
C4-C3	σ	1.968	C5-C4	σ*	0.041	2.64	1.22	0.051
-	-	-	C3-C2	σ*	0.034	3.94	1.27	0.063
-	-	-	C2-Br13	σ*	0.028	5.00	0.79	0.056
C3-C2	σ	1.978	C4-C3	σ*	0.042	3.12	1.26	0.056
-	-	-	C4-N7	σ*	0.021	2.11	1.25	0.046
C3-C2	π	1.711	C1-C6	π*	0.318	21.30	0.30	0.072
-	-	-	C5-C4	π*	0.472	14.41	0.30	0.061
C8-C9	σ	1.986	C10-C9	σ*	0.014	2.28	1.30	0.049
-	-	-	C8-N7	σ*	0.013	1.28	1.27	0.036
LPN7	σ	1.904	C5-C4	σ*	0.041	10.49	0.88	0.087
-	-	-	C8-C9	σ*	0.026	9.52	0.89	0.084
LPO11	σ	1.975	C4-C3	σ*	0.042	7.00	1.09	0.078
LPO11	π	1.836	C3-C2	π*	0.378	37.87	0.33	0.105
LPO11	n	1.531	C3-C2	σ*	0.034	5.98	1.03	0.079
LPBr13	σ	1.995	C1-C2	σ*	0.025	1.29	1.47	0.039
-	-	-	C3-C2	σ*	0.034	1.00	1.51	0.035
LPBr13	π	1.972	C1-C2	σ*	0.025	2.71	0.82	0.042
-	-	-	C3-C2	σ*	0.034	3.77	0.86	0.051
LPBr12	n	1.935	C3-C2	π*	0.378	9.90	0.30	0.053
LPBr12	n	1.970	C6-C5	σ*	0.034	3.23	0.82	0.046

LPBr12	n	1.945	C1-C6	π*	0.318	9.29	0.31	0.051

DIHQ(**2**)

Donor(i)	Type	ED/e	Acceptor(j)	Type	ED/e	E(2)[a]	E(j)-E(i)[b]	F(i,j)[c]
C9-C10	σ	1.980	C5-C6	σ*	0.035	4.92	1.21	0.069
C9-C8	σ	1.985	C9-C10	σ*	0.014	1.38	1.24	0.03
C5-C6	σ	1.975	C10-C5	σ*	0.025	3.62	1.20	0.059
-	-	-	C4-N7	σ*	0.025	3.90	1.15	0.060
C6-C1	σ	1.973	C10-C5	σ*	0.025	4.80	1.22	0.068
-	-	-	C5-C6	σ*	0.035	2.19	1.22	0.046
-	-	-	C2-C1	σ*	0.028	2.18	1.23	0.046
C6-C1	π	1.763	C3-C2	π*	0.367	13.87	0.29	0.059
C3-C2	σ	1.978	C4-N7	σ*	0.025	2.75	1.18	0.051
-	-	-	C2-C1	σ*	0.028	1.93	1.25	0.044
C3-C2	π	1.713	C6-C1	π*	0.307	22.70	0.30	0.074
LPC5	σ	1.013	C9-C10	π*	0.014	59.36	0.14	0.103
-	-	-	C6-C1	π*	0.025	57.98	0.14	0.099
LPN7	σ	1.907	C9-C8	σ*	0.027	10.14	0.84	0.084
-	-	-	C5-C4	σ*	0.046	11.15	0.84	0.087
LPO11	σ	1.976	C4-C3	σ*	0.044	7.40	1.04	0.079
LPI12	σ	1.993	C5-C6	σ*	0.035	1.28	1.10	0.034
LPI12	π	1.974	C5-C6	σ*	0.035	3.09	0.75	0.043
-	-	-	C6-C1	σ*	0.025	2.10	0.81	0.037
LPI12	n	1.955	C6-C1	π*	0.307	6.40	0.28	0.040
LPI13	π	1.975	C3-C2	σ*	0.034	3.41	0.79	0.047
LPI13	n	1.943	C3-C2	π*	0.367	7.41	0.26	0.043

[a]E(2) means energy of hyper-conjugative interactions (stabilization energy in kJ/mol)

[b]Energy difference (a..u) between donor and acceptor i and j NBO orbitals

[c]F(i,j) is the Fock matrix elements (a.u.) between i and j NBO orbitals

Table 3

NBO results showing the formation of Lewis and non-Lewis orbitals

DBHQ(**1**)

Bond(A-B)	ED/e[a]	EDA%	EDB%	NBO	s%	p%
πC1-C6	1.771	45.41	54.59	0.6739($sp^{1.00}$)C+	0.00	100.0
-	-0.287	-	-	0.7388($sp^{1.00}$) C	0.00	100.0
σC1-C2	1.971	49.49	50.51	0.7035($sp^{1.93}$)C+	34.17	65.79
-	-0.724	-	-	0.7107($sp^{1.58}$)C	38.68	61.28
σC4-C3	1.968	50.49	4951	0.7106($sp^{2.00}$)C+	33.27	66.68
-	-0.706	-	-	0.7036($sp^{1.82}$)C	35.42	64.54
σC3-C2	1.978	49.95	50.05	0.7068($sp^{1.61}$)C+	38.36	61.60
-	-0.758	-	-	0.7074($sp^{1.58}$)C	38.80	61.15
πC3-C2	1.711	43.63	56.37	0.6605($sp^{1.00}$)C+	0.00	100.0
-	-0.290	-	-	0.7508($sp^{1.00}$)C	0.00	100.0
σC8-C9	1.986	49.21	50.79	0.7015($sp^{1.65}$)C+	37.78	62.17
-	-0.715	-	-	0.7127($sp^{1.97}$)C	33.68	66.28
n1N7	1.904	-	-	$sp^{2.67}$	27.23	72.66
-	-0.366	-	-	-	-	-
n1O11	1.975	-	-	$sp^{1.31}$	43.30	56.64
-	-0.592	-	-	-	-	-
n2O11	1.836	-	-	$sp^{1.00}$	0.00	100.0
-	-0.321	-	-	-	-	-
n3O11	1.531	-	-	$sp^{3.63}$	21.58	78.31
-	-0.466	-	-	-	-	-
n1Br13	1.995	-	-	$sp^{0.16}$	86.49	13.51
-	-0.947	-	-	-	-	-
n2Br13	1.972	-	-	$sp^{99.99}$	0.16	99.84
-	-0.292	-	-	-	-	-
n3Br13	1.935	-	-	$sp^{1.00}$	0.00	100.0
-	-0.291	-	-	-	-	-
n2Br12	1.970	-	-	$sp^{99.99}$	0.02	99.98

-	-0.301	-	-	-	-	-
n3Br12	1.945	-	-	$sp^{1.00}$	0.00	100.0
-	-0.299	-	-	-	-	-

DIHQ(**2**)

Bond(A-B)	ED/e[a]	EDA%	EDB%	NBO	s%	p%
σC9-C10	1.980	49.57	50.43	0.7041($sp^{1.76}$)C+	36.22	63.78
-	-0.735	-	-	0.7101($sp^{1.80}$)C	35.72	64.28
σC9-C8	1.985	50.69	49.31	0.7119($sp^{1.97}$)C+	33.67	66.33
-	-0.716	-	-	0.7022($sp^{1.65}$)C	37.67	62.33
σC5-C6	1.975	51.04	48.96	0.7144($sp^{1.88}$)C+	34.75	65.25
-	-0.730	-	-	0.6997($sp^{1.53}$)C	39.56	60.44
σC6-C1	1.973	50.01	49.99	0.7072($sp^{1.50}$)C+	40.01	59.99
-	-0.749	-	-	0.7071($sp^{1.71}$)C	36.87	63.13
πC68-C1	1.763	55.20	44.80	0.7430($sp^{1.00}$)C+	0.00	100.00
-	-0.294	-	-	0.6693($sp^{1.00}$)C	0.00	100.00
σC3-C2	1.978	50.13	49.87	0.7080($sp^{1.58}$)C+	38.72	61.28
-	-0.760	-	-	0.7062($sp^{1.55}$)C	39.23	60.77
πC3-C2	1.713	44.18	55.82	0.6647($sp^{1.00}$)C+	0.00	100.00
-	-0.299	-	-	0.7472($sp^{1.00}$)C	0.00	100.00
n1C5	1.013	-	-	$sp^{1.00}$	0.00	100.00
-	-0.137	-	-	-	-	-
n1N7	1.907	-	-	$sp^{2.48}$	28.74	71.26
-	-0.368	-	-	-	-	-
n1O11	1.976	-	-	$sp^{1.21}$	45.34	54.66
-	-0.580	-	-	-	-	-
n1I12	1.993	-	-	$sp^{0.11}$	89.74	10.26
-	-0.625	-	-	-	-	-
n2I12	1.974	-	-	$sp^{99.99}$	0.11	99.89
-	-0.279	-	-	-	-	-
n3I12	1.955	-	-	$sp^{1.00}$	0.00	100.00
-	-0.276	-	-	-	-	-

n2I13	1.975	-	-	$sp^{99.99}$	0.32	99.68
-	-0.26	-	-	-	-	-
n3I13	1.943	-	-	$sp^{1.00}$	0.00	100.00
-	-0.266	-	-	-	-	-

[a]ED/e is expressed in a.u.

Table 4

PASS prediction for the activity spectrum of the title compounds, Pa represents probability to be active and Pi represents probability to be inactive

DBHQ(1)

Pa	Pi	Activity
0.945	0.003	Antiseptic
0.917	0.002	Antiprotozoal
0.911	0.003	Dehydro-L-gulonate decarboxylase inhibitor
0.907	0.004	Antiinfective
0.906	0.007	Aspulvinone dimethylallyl transferase inhibitor
0.894	0.003	Glutathione thiolesterase inhibitor
0.868	0.004	Alkane 1-monooxygenase inhibitor
0.855	0.003	Corticosteroid side-chain-isomerase inhibitor
0.826	0.003	Cis-1,2-dihydro-1,2-dihydroxynaphthalene dehydrogenase Inhibitor
0.825	0.009	Glycosylphosphatidylinositol phospholipase D inhibitor

DIHQ (2)

Pa	Pi	Activity
0.966	0.002	Antiprotozoal
0.911	0.003	Dehydro-L-gulonate decarboxylase inhibitor
0.894	0.003	Glutathione thiolesterase inhibitor
0.868	0.004	Alkane 1-monooxygenase inhibitor
0.855	0.003	Corticosteroid side-chain-isomerase inhibitor
0.826	0.003	Antiprotozoal
0.851	0.003	Cis-1,2-dihydro-1,2-dihydroxynaphthalene dehydrogenase Inhibitor
0.825	0.009	Glycosylphosphatidylinositol phospholipase D inhibitor
0.818	0.003	Hydroxylamine reductase (NADH) inhibitor
0.823	0.010	Glucose oxidase inhibitor

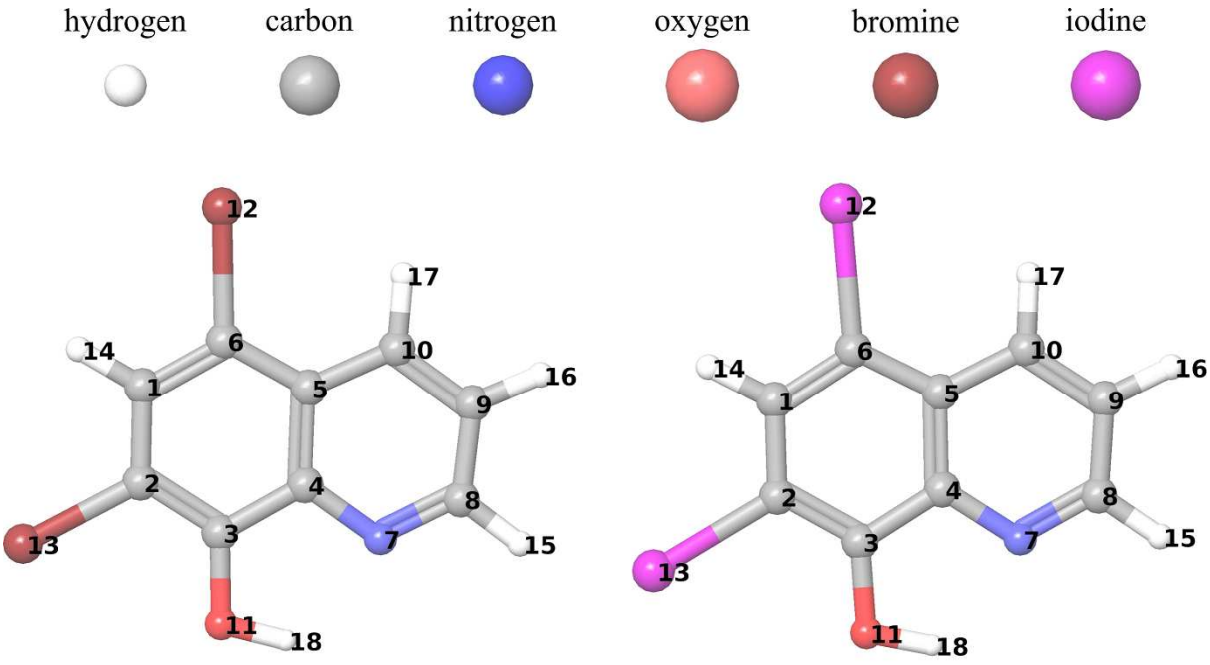

1 **2**

1 **2**

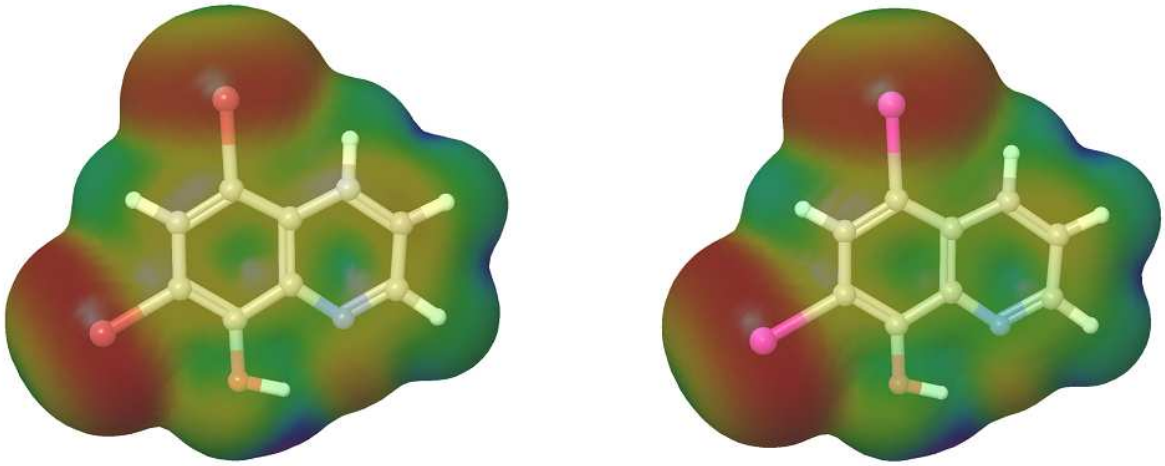

min: 199.84 max: 384.29 min: 181.91 max: 382.03

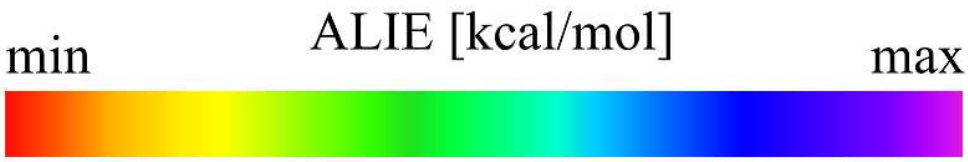

1

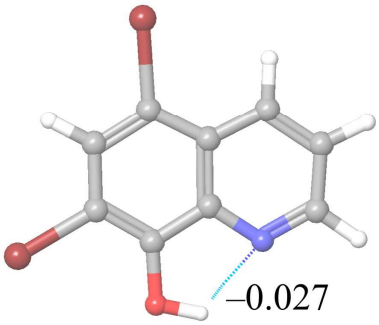

2

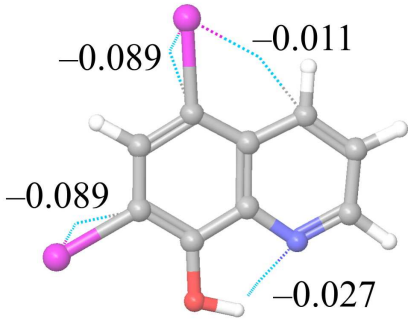

	f^+	f^-
1	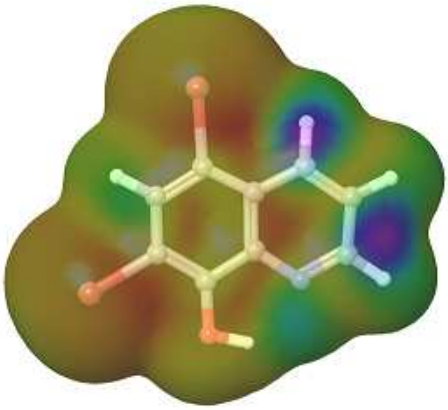	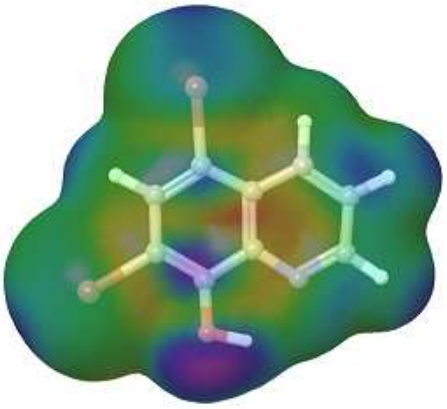
2	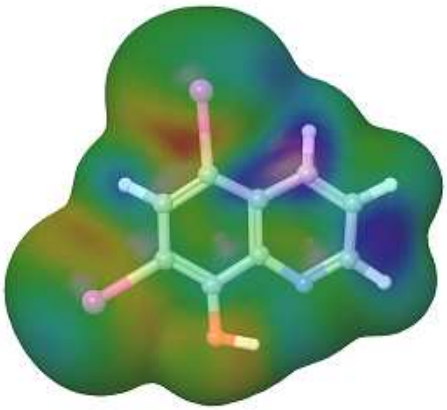	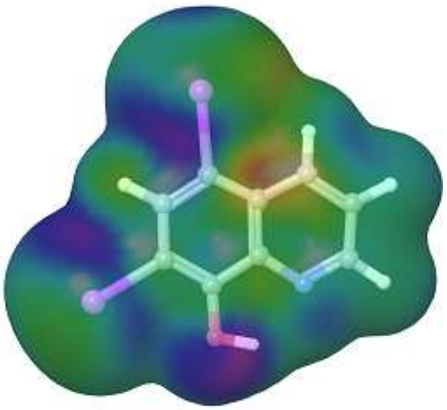

1 **2**

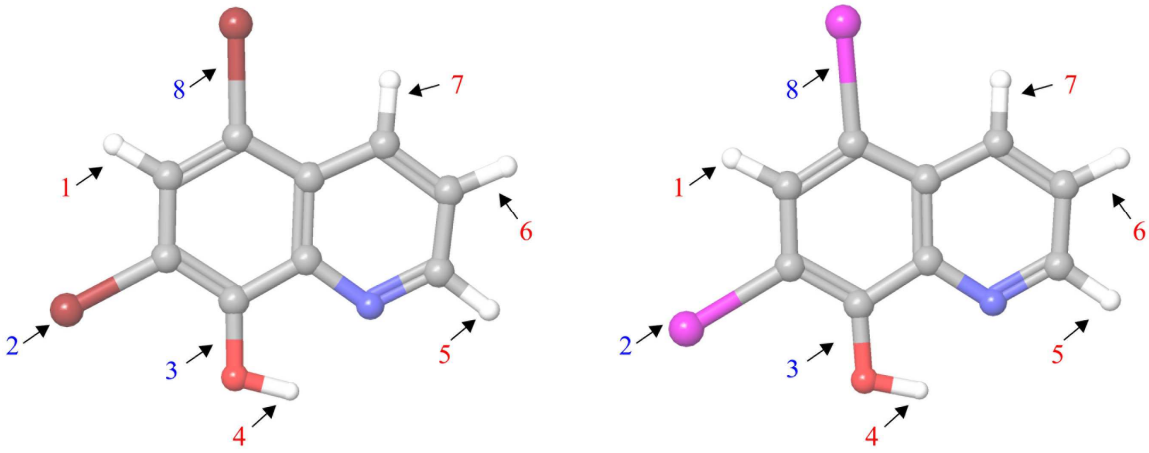

Bond number	1	2
1	118.23	116.28
2	72.19	65.00
3	119.48	119.35
4	93.35	93.30
5	112.60	112.58
6	118.97	118.89
7	117.82	117.00
8	71.54	63.39

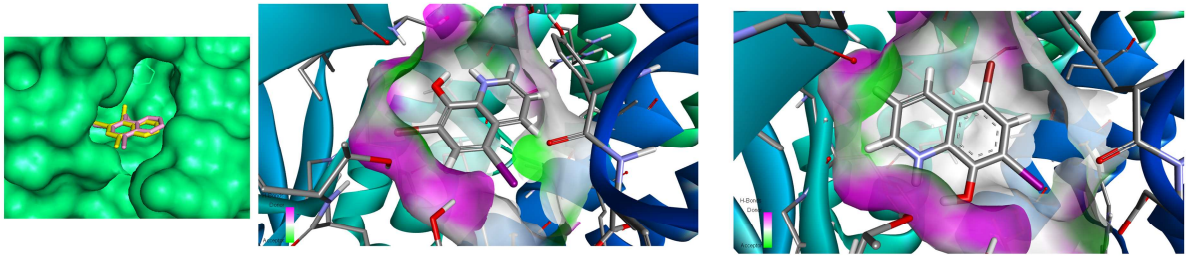

(A) (B) (C)

- Spectroscopic properties of two 8-hydroxy-quinoline derivatives were investigated,
- Important reactive centers have been identified by DFT calculations,
- MD simulations were used in order to investigate reactivity with water molecules,
- Docking study revealed significant binding properties against 3QGT protein.